Original paper

Crystal structure of the uranyl–molybdate mineral calcurmolite $Ca[(UO_2)_3(MoO_4)_2(OH)_4](H_2O)_{\sim 5.0}$: insights from a precession electron-diffraction tomography study

Gwladys STECIUK[1*], Radek ŠKODA[2], Jan ROHLÍČEK[1], Jakub PLÁŠIL[1]

[1] *Institute of Physics, Academy of Sciences of the Czech Republic v.v.i, Na Slovance 2, 182 21 Prague 8, Czech Republic; steciuk@fzu.cz*
[2] *Department of Geological Sciences, Masaryk University, Kotlářská 2, 611 37 Brno, Czech Republic*
[*] *Corresponding author*

Calcurmolite is a rare supergene U mineral formed during the alteration–hydration weathering of uraninite and hypogene Mo minerals; its structure has remained unsolved owing to a lack of crystal material suitable for conventional structure analysis. Here, single-crystal precession electron-diffraction tomography shows the calcurmolite (Rabejac, France) structure to be modulated; it is triclinic, crystallizing in the super-space group $P1(\alpha 00)0$, with a = 3.938 Å, b = 11.26 Å, c = 14.195 Å, α = 84.4°, β = 112.5°, γ = 133.95° and has a modulation vector q = 0.4 ***a****. Due to the poor quality of diffraction data, only a kinematical refinement was undertaken, although final results were reasonable: R_{obs}/R_{all} = 0.3825/0.3834 for 3953/17442 observed/all reflections. The structure of calcurmolite is based upon the infinite uranyl–molybdate sheets with baumoite topology (U : Mo ratio = 1.5) and an interlayer of 6-coordinated Ca^{2+} cations with interstitial H_2O (ligands are apical uranyl O atoms and molecular H_2O). Adjacent sheets are linked *via* Ca–O, as well as H-bonds. The structure formula, based on assumed occupancies in the supercell $5a \times b \times c$, is $Ca[(UO_2)_3(MoO_4)_2(OH)_4](H_2O)_{\sim 5.0}$ (for Z = 4).

Keywords: calcurmolite, uranyl–molybdate, crystal structure, modulation, baumoite topology, precession electron diffraction
Received: 18 November 2019; accepted: 5 March 2020; handling editor: F. Laufek
The online version of this article (doi: 10.3190/jgeosci.297) contains supplementary electronic material

1. Introduction

Uranyl–molybdates are uncommon alteration products that result from the weathering of uraninite UO_{2+x}, associated with some hypogene molybdenum-containing minerals, such as molybdenite MoS_2, or its Fe-rich variety, called 'femolite' $(Mo,Fe)S_2$. The latter femolite is less stable under oxidizing conditions (Krivovichev and Plášil 2013). Currently, only nine uranyl–molybdates are known from oxidized parts of uranium deposits worldwide; nevertheless, their crystal chemistry is particularly interesting as it diverges from other known U^{6+}-containing compounds (Burns 2005). The family of synthetic molybdates is considerably broad (*e.g.* Krivovichev and Burns 2000a, b, 2001a, b, 2002a, b, c, d; Krivovichev et al. 2002); it may be speculated that some of these will be discovered in nature.

Originally, calcurmolite was described by Rudnitskaya (1959) as a new mineral from the Kadjaran ore field, the Kafan region, Armenia, under the name 'kadjaranite'. Later on, it was found by Fedorov (1963) and Skvortsova et al. (1969) in Kazakhstan at U–Mo deposits, and then reported by Deliens (1992) from Rabejac, France. Sidorenko et al. (2005) presented new chemical data from electron microprobe, infrared (IR) spectroscopy and powder X-ray diffraction for samples from Kazakhstan and Armenia. They demonstrated that calcurmolite forms fine intergrowths with uranophane and uranocircite, which makes its detailed study difficult. On the basis of IR spectra, Sidorenko et al. (2005) concluded that, similar to umohoite, iriginite and mourite, calcurmolite does not contain $(MoO_4)^{2-}$ tetrahedral oxyanions, but Mo^{6+} appears in octahedral coordination. This conclusion was confirmed by Frost et al. (2008) by Raman spectroscopy studies of calcurmolite. Calcurmolite minerals of different origins were already reported as poorly crystallized phases by Deliens (1992) and Dal Bo (2018). Up to now, reliable structure data were lacking for this mineral and the chemical formula represented only an uncertain estimate.

Here we report the crystal structure of calcurmolite for the first time based on a precession electron-diffraction tomography study carried out on a calcurmolite sample from the Lodève Basin in France. This method is a good alternative to single-crystal X-ray diffraction for samples like calcurmolite made of small crystals (*c.* 1–5 μm). Moreover, despite the generally poor crystallization ability of the mineral, small parts of crystals giving satisfying diffraction signal were found at the nanoscale allowing a structural determination.

Fig. 1 Calcurmolite specimen. Yellow calcurmolite with orange to reddish-orange umohoite on alteration crust from Rabejac, France. Horizontal width of the picture is 3 mm (photo S. Wolfsried).

2. Occurrence

The specimen of calcurmolite investigated here originates from the Rabejac deposit in the Lodève Basin, located in the southern part of Massif Central, France. More detailed information about the locality, and its mineralogy and geology, can be found in Dal Bo (2018). Calcurmolite is present as bright yellow nodules resembling mimosa flowers constituted by a radial aggregation of tiny prismatic crystals with a section of 1–5 μm (Fig. 1). In the studied sample, calcurmolite is associated with reddish-brown umohoite and pale yellow uranophane-β. The sample matrix consists of a fine-grained sandstone with the uranyl minerals mentioned above being scattered on the surface.

3. Chemical composition

The chemical composition of calcurmolite was determined using a Cameca SX 100 electron microprobe operated in WDS mode. An operating voltage of 15 kV, beam current of 10 nA and a 10 μm beam diameter and the following X-ray lines and standards were used: K_α lines: Na (albite), K (orthoclase), Ca (andradite), Al (gahnite), V (vanadinite), Fe (almandine); L_α lines: Mo (metallic Mo), As (lammerite); M_α lines: Pb (vanadinite); M_β lines: U (UO_2). Other elements were sought but not detected. Peak counting times were 10–20 s and the counting time for the background was 50 % of that of the peak. Matrix effects were accounted for using the *PAP* correction routine (Pouchou and Pichoir 1985). Because of the paucity of pure material required for direct H_2O determination, molecular H_2O was calculated based on stoichiometric constrains. Chemical microanalysis revealed the rather homogeneous nature of the specimen. The empirical formula, calculated as the mean of 13 representative points (Tab. 1), is $(K_{0.005}Na_{0.005})_{\Sigma 0.01}Ca_{0.16}[(UO_2)_{0.6}O_{1.6}Mo_{0.395}(OH)_{0.80}](H_2O)_{\sim 1.0}$ based on 0.6 U *apfu*; stoichiometry derived from the modulated structure with $Z = 4$. In the $5a \times b \times c$ supercell, the composition becomes $(K_{0.025}Na_{0.025})_{\Sigma 0.05}Ca_{0.8}[(UO_2)_3O_8Mo_{1.975}(OH)_4](H_2O)_{\sim 5.0}$ for $Z = 4$. The ideal chemical formula in the supercell is $Ca[(UO_2)_3(MoO_4)_2(OH)_4](H_2O)_{\sim 5}$.

4. Structure determination

4.1. Powder X-ray diffraction (PXRD)

For the collection of powder X-ray diffraction data, the sample was ground and placed to the 0.3 mm borosilicate-glass capillary. Powder diffraction data were collected in Debye–Scherrer transmission at

Tab. 1 Chemical composition of calcurmolite from WDS (in wt. % oxides)

	Mean (n = 13)	Range	SD
CaO	3.49	3.37–3.63	0.08
Na_2O	0.04	0.00–0.12	0.05
K_2O	0.13	0.00–0.26	0.09
MoO_3	22.17	21.10–23.11	0.57
UO_3	67.18	64.48–68.13	0.90
H_2O (calc.)	9.94*		
Total	102.50		

* calculated from the structure
SD – standard deviation

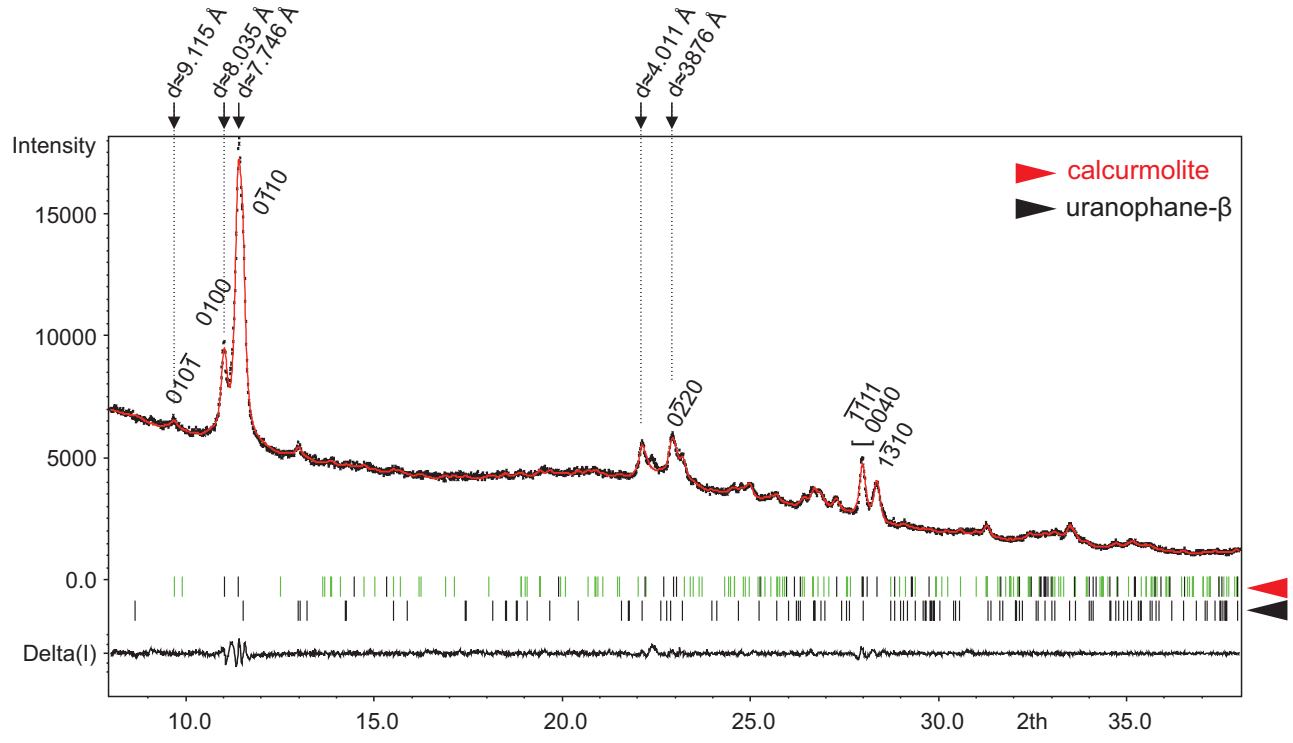

Fig. 2 Le Bail fit of the powder X-ray diffraction data of calcurmolite ($P1(\alpha 00)0$) indicating the presence of uranophane-β. The black and green sticks indicate the main and the first-order satellite reflections of calcurmolite, respectively. R_p = 0.0158, wR_p = 0.0209 and Goodness of fit, *GOF* = 0.0139. The most characteristic interplanar distances reported in the literature are indicated above the diagram.

150 K on a Empyrean of PANalytical (λ (CuK_α) = 1.54184 Å) powder diffractometer, equipped with the focusing mirror, capillary holder and PIXcel^{3D} detector. The most characteristic calcurmolite peaks are found for interplanar distances of 9.115, 8.03, 7.746, 4.01, and 3.876 Å (Fig. 2). The powder X-ray diffraction pattern shows a lot of similarities with previous study of calcurmolite from Rabejac (Deliens 1992) and from Kazakhstan and Armenia (Sidorenko et al. 2005), but cannot be considered as being identical. The strongest similarities are found with the second sample from Kazakhstan (Sidorenko et al. 2005) where all the characteristic peaks mentioned above are present with comparable relative intensities. This observation is surprising as the composition of calcurmolite from Rabejac in this study is closer to other sample of the same origin (Deliens 1992) than calcurmolite from Kazakhstan (Sidorenko et al. 2005).

The X-ray powder pattern did not provide any further, useful structural information due to the poorly crystalline nature of calcurmolite as well as the presence of significant quantities of uranophane-β. Though, the powder X-ray diffraction data were used to refine the unit cell parameters determined by electron diffraction (see later) and to validate that the crystals measured at the nanoscale were representative of the mineral.

4.2. Precession electron-diffraction tomography (PEDT)

As the low crystallinity and the size of calcurmolite crystals prevented single-crystal X-ray structure studies (all performed attempts failed), structure data were obtained from electron-diffraction and collected with a FEI Tecnai 20 transmission-electron microscope (TEM, acceleration voltage of 200 kV, LaB_6) using a Gatan cryo-transfer holder. For TEM investigations, a small portion of calcurmolite crystals was mildly crushed without solvent and deposited on a Cu-grid with a thin film of holey amorphous carbon. The grid was plunged into liquid nitrogen and then transferred to the TEM. Precession electron-diffraction tomography (PEDT) data sets of non-oriented patterns were collected at 100 K on several crystals (eight data sets) with the precession device Nanomegas Digistar and a side-mounted CCD camera Olympus Veleta with 14-bit dynamic range (Fig. 3a). The precession angle was set to 1° and a tilt step to 1° as well. A condenser aperture of 10 mm and a low illumination setting (spot size 8) were used to reduce the electron dose.

The PEDT data sets were analysed using programs PETS2.0 (Palatinus et al. 2019) and Jana2006 (Petříček et al. 2014). Albeit the crystals were poorly crystalized, at the nanoscale, a few better-crystallized areas of crystals

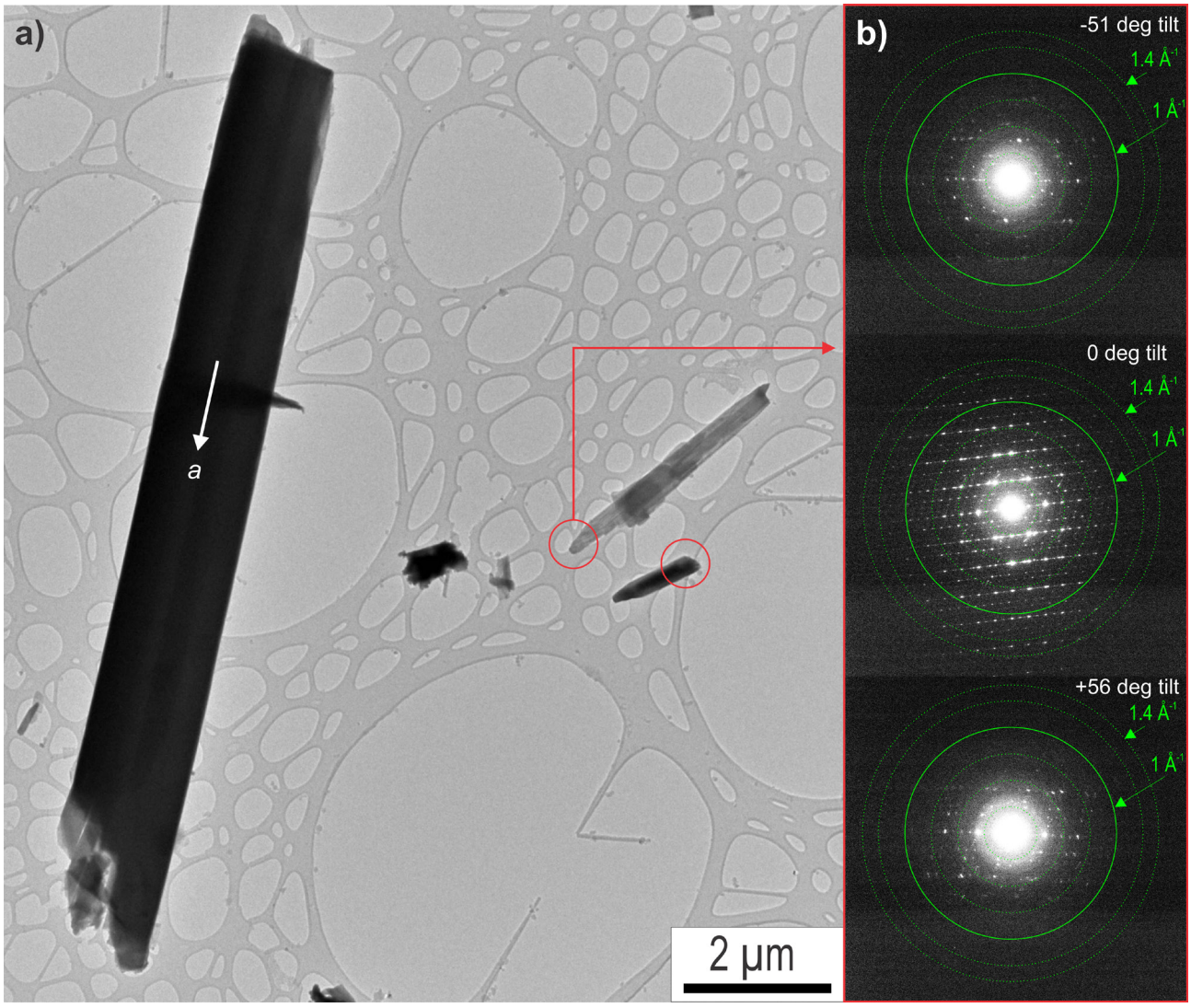

Fig. 3a – Needle-like calcurmolite crystals. The red circles represent the area selected for the PEDT experiments. **b** – For one data set the resolution rings are represented at high rotation angles of the goniometer (–51 and +56 deg) and for the preferential orientation (0 degree rotation). The resolution of g = 1.4 Å^{-1} corresponds to the maximum diffraction vector used by default in the data reduction.

were discovered making structural analysis possible by combining the two best data sets (Tab. 2). Only two of the eight measured data sets were used in the structural analysis because of limitations present in PEDT data. First, despite that the ordering along ***a**** is well visible on *h*0*l*m, as soon as the crystal was rotated during the PEDT experiments, diffuse scattering appeared along the stacking direction *b** (Figs 3b and 4b) and the resolution was significantly lowered. Moreover, because of the preferred orientation of needle-like crystals on the flat grid (Fig. 3a), the data completeness is limited to 76 % for a sin θ/λ = 0.7 Å^{-1} resolution. Combining more data sets (four were of acceptable quality) did not improve the data completeness and drastically increased the R_{int} value.

The reciprocal space was first indexed using the superspace formalism in a standard triclinic unit cell: a = 3.938 Å, b = 8.15 Å, c = 13.14 Å, α = 104.7°, β = 96.4°, $\gamma \approx 90°$, V = 409.7 Å^3 and a modulation vector $\boldsymbol{q}$ = 0.4 ***a**** + 0.8 ***b**** + 0.4***c**** with satellite reflections up to 2nd order (Fig. 4a). In Fig. 4a the reciprocal space is projected into one unit cell to show that, despite the presence of diffuse features and the signal coming from other orientations, most of the reflections are indexed. However, because the completeness is low and the structure needs to be manually interpreted layer by layer, a non-standard choice was preferred with the following parameters: a = 3.938 Å, b = 11.26 Å, c = 14.195 Å, α = 84.4°, β = 112.5°, γ = 133.95° and a modulation vector q = 0.4 ***a**** with satellite reflections up to 2nd order (V = 409.72 Å^3) (Fig. 4a). With these settings the layers can be represented in the supercell 5$a \times b \times c$ in (a, c) planes, the modulation occurs along a* and the layers are stacked following the *b*-axis. Based on few peaks from PXRD patterns, Dal Bo (2018), Deliens (1992) and Sidorenko et al. (2005) sug-

gested that calcurmolite could be indexed in a monoclinic or pseudo-orthorhombic unit cell. From PEDT single-crystal data, only triclinic unit cells are found. The intensity integration was performed using the new options available in PETS2.0 using the non-standard settings. The experimental intensity profile (rocking curve) is fitted using several parameters including the rocking curve width (*RC width* = 0.017 Å^{-1}) and the apparent mosaicity (*mosaicity* = 0.25°) (for detailed information, see Palatinus et al. 2019). The values of the apparent mosaicity and RC width are very high for calcurmolite data because of the presence of the disorder features along *b** and the high mosaicity of the crystals (for well crystallized crystals measured with the same microscope: RC width ≤0.003 Å^{-1} and mosaicity ≤0.05°).

Tab. 2 Summary of data collection conditions and refinement parameters for calcurmolite

Structural formula in the modulated cell Structural formula in the supercell*	$Ca_{0.2}[(UO_2)_{0.6}O_{1.6}Mo_{0.4}(OH)_{0.8}](H_2O)_{\sim 1.0}$ $Ca_1[(UO_2)_3O_8Mo_2(OH)_4](H_2O)_{\sim 5.0}$
Unit-cell parameters (PEDT) At 100 K	a = 3.938 Å, b = 11.26 Å, c = 14.195 Å, α = 84.4°, β = 112.5°, γ = 133.95°, $\boldsymbol{q}$ = 0.4 $\boldsymbol{a}$*
Unit-cell parameters (PXRD) At 150 K	a = 3.927(2) Å, b = 11.500(4) Å, c = 14.175(2) Å, α = 85.20(2)°, β = 111.70(2)°, γ = 134.05(2)°, $\boldsymbol{q}$ = 0.4 $\boldsymbol{a}$*
V (100K)	409.7(2) Å^3
Z	4
Density [g.cm^{-3}] (from PEDT)	4.2124
Space group	$P1(\alpha 00)0$
Temperature	100 K
Transmission electron microscope	FEI Tecnai 02
Radiation (wavelength)	electrons, (0.0251 Å)
Resolution	0.1–0.7 Å^{-1}
Limiting Miller indices	$-6 < h < 6$, $-15 < k < 15$, $-19 < l < 19$, $-2 < m < 2$
No. of independent reflections (obs/all) – kinematic	all : 3953/17442 main : 1343/3501 order 1 : 1736/6943 order 2 : 874/6998
Coverage for $sin\theta/\lambda$ = 0.7 Å^{-1}	76.06 %
R_{int} (obs/all) – kinematic	0.2374/0.3901
Redundancy	1.715
R, wR (obs) (kinematical)	all : 0.3825/0.3834 main : 0.3313/0.3445 order 1 : 0.3887/0.4136 order 2 : 0.5441/0.6170
N refined parameters	100

*5$a \times b \times c$ supercell

The structure was solved using the charge-flipping algorithm (Palatinus and Chapuis 2007) in the superspace group (SSG) P–1(α00)0 and later refined in the SSG $P1(\alpha 00)0$. Because of all the limitations presented previously, the structure solution did not arise directly from the charge-flipping algorithm; the initial result, a 3D electrostatic potential map (e-map) represented as isosurfaces, had to be interpreted manually (Fig. 5). The e-map shows a structure resulting from the alternation of two different layers: the first having strong electrostatic potentials attributed to a uranium–molybdenum layer: the second containing calcium and H_2O that is not resolved enough to be interpreted directly from the e-map (Fig. 5a). In the U–Mo layer (Fig. 5b), by lowering the isosurfaces level of the potential map to 1σ[ΔV(r)], the visible oxygen positions define two possible coordination polyhedra around the cations: an octahedral coordination and a pentagonal bipyramid coordination. These are characteristic of Mo^{6+}(Mo^{5+}) and U^{6+} environments, respectively (Fig. 5b). Following these observations, in the modulated description (SSG P–1(α00)0), Mo and U share the same two cationic sites and their ordering is described using a discontinuous crenel-like modulation function with Δ (U1,2) = 0.6 and Δ (Mo1,2) = 0.4, the width of the crenels (crenel-like; Petříček et al. 2016) associated with one harmonic function. The apical oxygen sites (Oa1, Oa2, Ob1 and Ob2) functions as well as the O3 and O4 atoms located within the U–Mo plane are defined without modulation due to lack of information from the data. The additional oxygen sites O5a, O5b, O5c and O5d of the U–Mo plane are described using crenel functions. The position of the atomic sites described with crenel functions as a function of t is shown in Fig. 6 in the final superspace group $P1(\alpha 00)0$. The ratio Mo/(U + Mo) = 2/5 corresponding directly to the α component of the modulation vector shows that the origin of the modulation is explained by the ordering of uranium and molybdenum along ***a****. The refinement of the initial model was performed in the SSG $P1(\alpha 00)0$ using the kinematical approximation against PEDT data in order to reveal the topology of the Ca–O layer. In the case of calcurmolite, the poor quality of the data as well as the large number of refined parameters prevented the use of the dynamical refinement (Palatinus et al. 2015a, b). Indeed, the presence of disorder reduces the dynamics effects and hence makes refinement using the kinematical approximation relevant. Distance restrictions were applied to maintain the polyhedra of the U–Mo layer. The calcium-based layer was revealed from the difference–Fourier map, with two Ca sites in the 6- and 7-coordination, and four anion sites (occupied by molecular water) (Fig. 7). The occupancies of the Ca sites

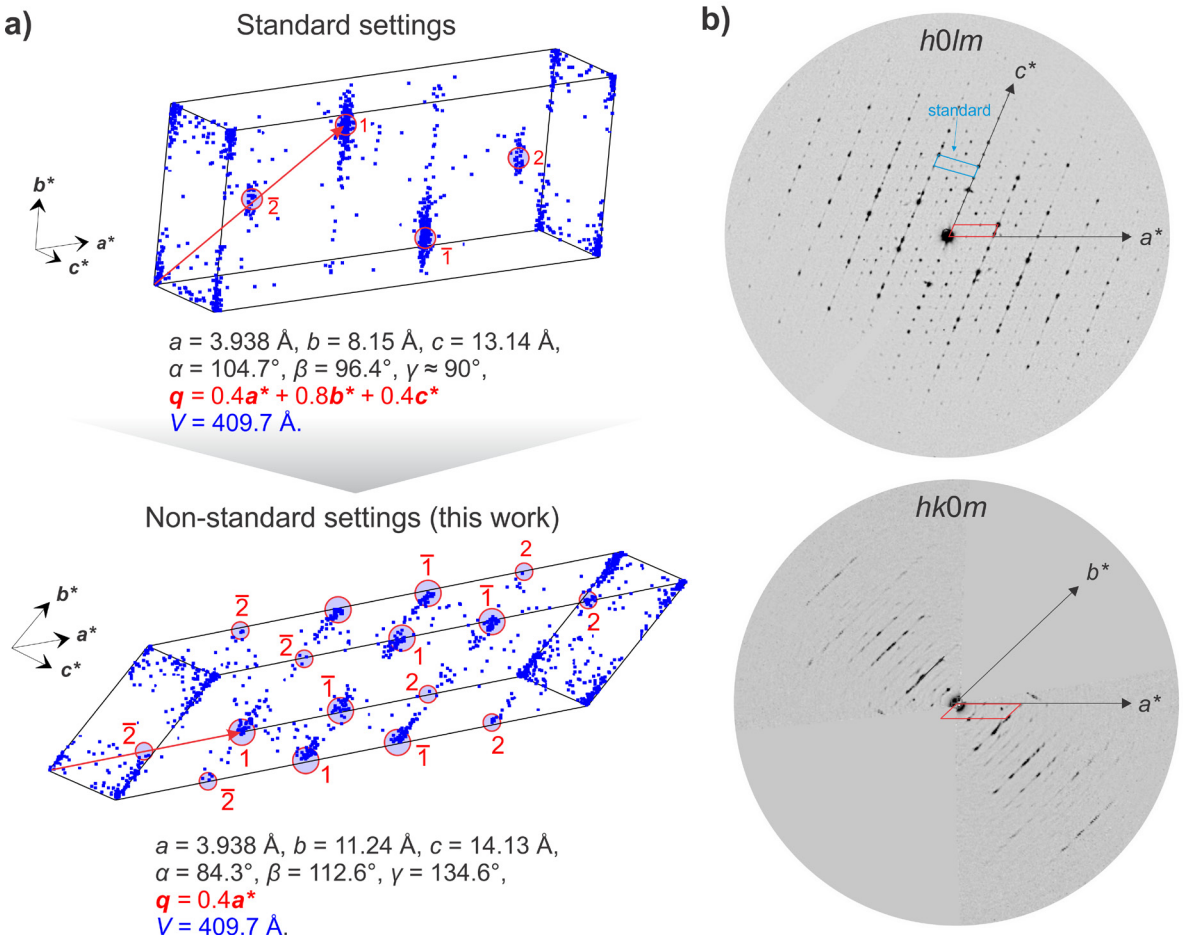

Fig. 4a – Projection of the reciprocal space into one modulated unit cell and two orders of satellite reflections for the standard settings and the settings used in this work. **b** – Two reciprocal space sections showing the ordering along the *a* axis on *h*0*l*m and the low resolution together with the disorder along the stacking direction ***b**** visible on *hk*0*m*.

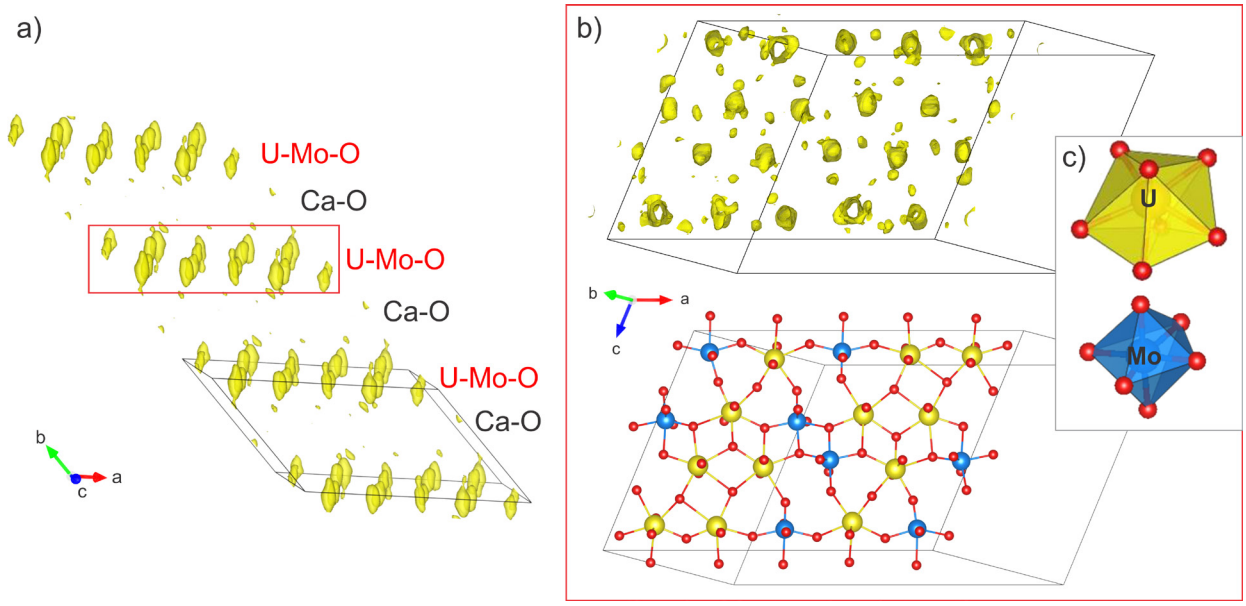

Fig. 5a – Isosurfaces of the 3D electrostatic potential map (e-map) extended along the stacking direction. Isosurface levels are 2σ[ΔV(r)]. **b** – [010]* e-map projection of the layer (1σ[ΔV(r)]) containing uranium, molybdenum and oxygen with its interpretation. The layer model is represented in the supercell 5*a* × *c*. **c** – Coordination polyhedra of U^{6+} and Mo^{6+}.

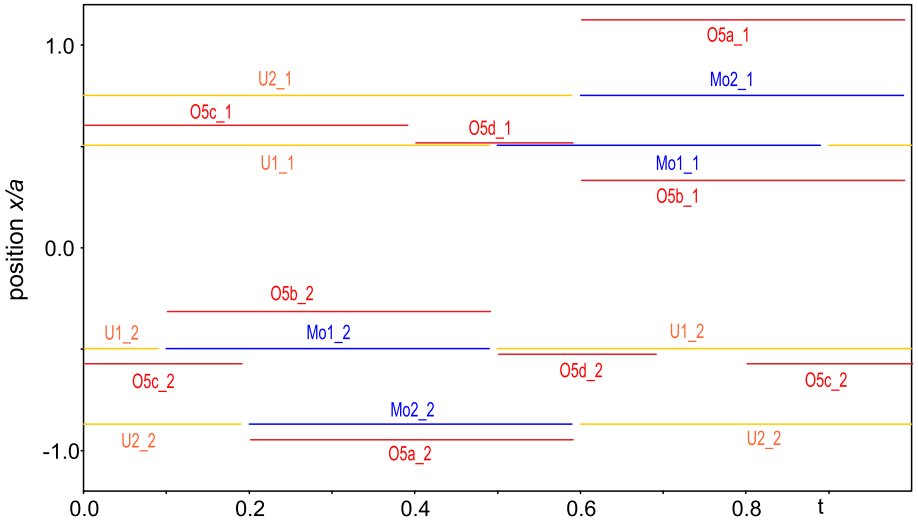

Fig. 6 Positional parameter *x/a* as a function of *t* for the atoms described using crenel-like functions in the SSG *P*1(*α*00)0.

were set according to the result of the chemical analysis in order to maintain the U : Mo : Ca ratio of 3 : 2 : 1. No modulation was applied to the atoms of the Ca–O layer as the refinement of this layer is not sensitive from our data. From the first refinement an insight of the calcium–water layer topology was revealed from the difference–Fourier map but it cannot be refined or described with accuracy. The final refinement leads to R_{obs}/R_{all} = 0.3825/0.3834 for 3953/17442 observed/all reflections (see Tab. 2). These values can be considered reasonable for the kinematical refinement of a modulated structure from electron-diffraction data (Boullay et al. 2013; Palatinus et al. 2015b; Steciuk et al. 2016). The refined structure is displayed on the Fig. 8. The results of the refinement are given in the Tab. 2 and the cation–oxygen distances, as a function of *t*, are presented in Fig. 9. The average bond valences for uranium are *BV*(U1_1) = 6.146(5), *BV*(U1_2) = 6.404(8), *BV*(U2_1) = 6.196(7) and *BV*(U2_2) = 6.011(6) vu.

5. Description of the structure

The structure of calcurmolite contains four symmetrically-distinct U sites, four Mo sites, two Ca sites and 24 O sites. In the structure of calcurmolite, all U is found to be hexavalent, occurring in pentagonal bipyramidal coordination with two strong U≡O bonds, (*i.e.* forming uranyl ion $(UO_2)^{2+}$) and five weaker bonds distributed in the equatorial plane (Figs 5b and 8; Tab. 3). The four symmetrically-distinct Mo sites are [6]-coordinated in the form of irregular, distorted octahedra (Fig. 5b and 8). The Mo1_1 and Mo1_2 (and Mo2_1 with Mo2_2) polyhedra share a common edge to form $Mo_2\varphi_{10}$ dimers. The calcurmolite structure is based upon uranyl–molybdate sheets. The fundamental building blocks of those sheets are two trimers (I and II) of edge-sharing polyhedral composed respectively by two U1_1 and one U1_2 polyhedra (trimer I) and two U2_1 and one U2_2 polyhedra (trimer II) (Fig. 8). They form the six-membered clusters by sharing a common edge with other trimer (Fig. 8). These clusters are connected through the O5c (O5c_1 and O5c_2) equatorial atom of the U bipyramid to form irregular chains propagated along [–101]. These chains of polyhedra are connected through $Mo_2\varphi_{10}$ dimers in a stair-case way. Sheets found in the structure of calcurmolite are of the same topology as observed in the structure of baumoite (Elliot et al. 2019).

Adjacent sheets are separated from each other at interplanar distance of 7.5 Å. Between the sheets are two symmetrically independent Ca atoms and four symmetrically independent H_2O molecules (associated with Ow1_1, Ow1_2 and Ow2_1 and Ow2_2 atoms). The coordination of Ca atoms in the structure of calcurmolite is [6]. Most probably, Ow1_1 and Ow1_2 are transformer H_2O group, with [3]-coordinated O atom, while Ow2_1 and Ow2_2 are non-transformer H_2O group, with at least [4]-coordinated O atom (typology of H_2O after Hawthorne and Schindler 2008).

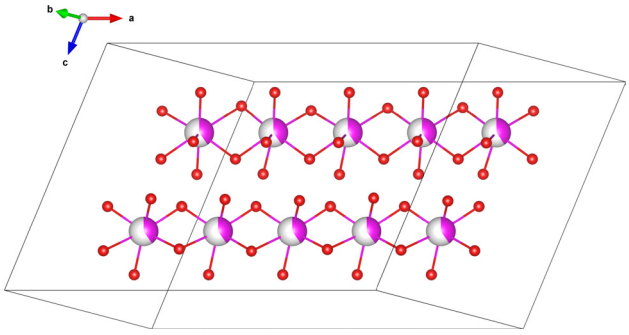

Fig. 7 Topology of the calcium–oxygen layer in the supercell revealed from the difference Fourier map after the kinematical refinement against PEDT data.

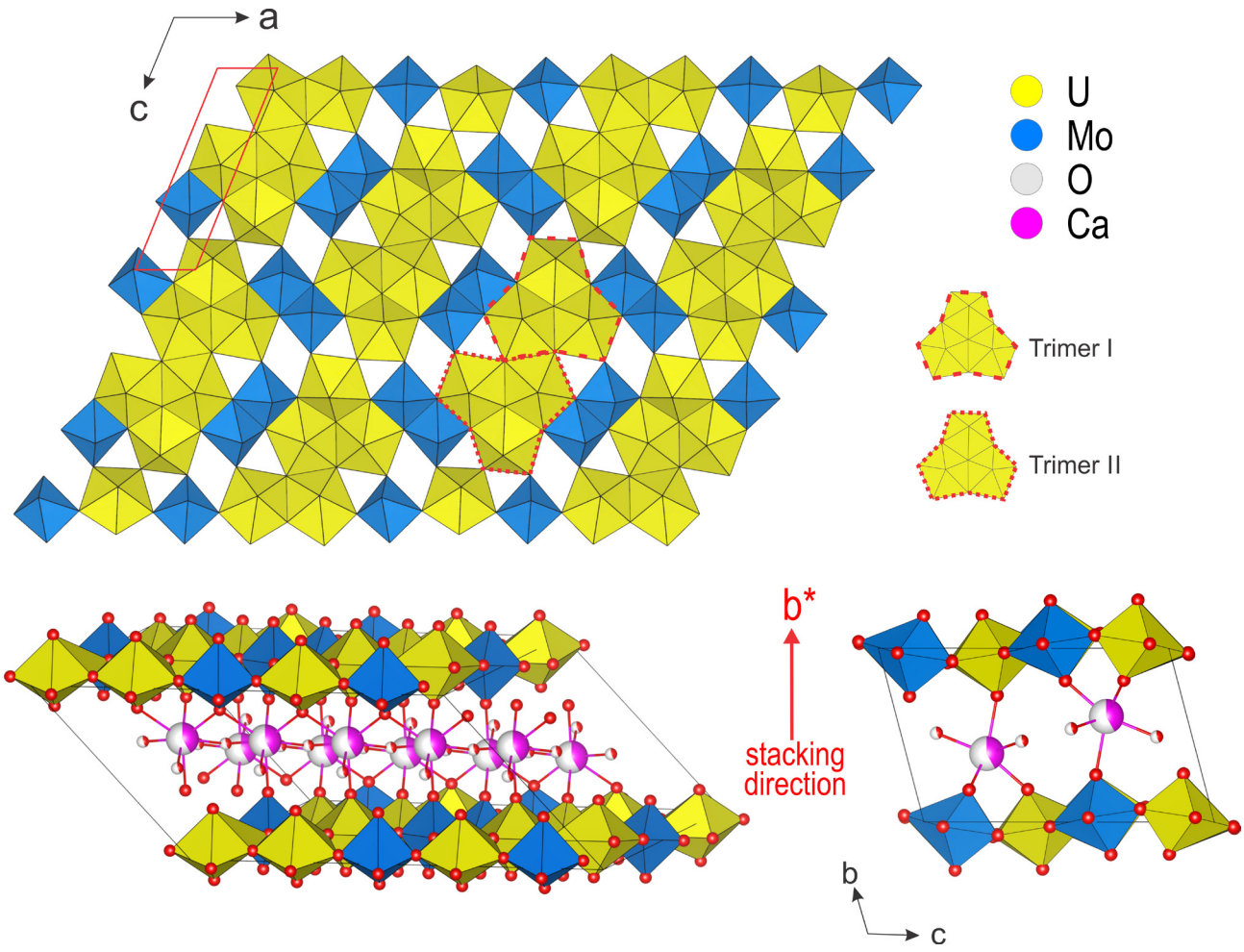

Fig. 8 Topology of the U–Mo layer and representation of the complete structure in the supercell $5a \times b \times c$.

The structure formula based on assumed occupancies is $Ca_{0.2}[(UO_2)_{0.6}(MoO_4)_{0.4}(OH)_{0.8}](H_2O)_{\sim 1.0}$, $Z = 4$ in the modulated unit cell. In the supercell $5a \times b \times c$ giving a complete overview of the topology, the formula becomes $Ca[(UO_2)_3(MoO_4)_2(OH)_4](H_2O)_{\sim 5.0}$. In his paper, Deliens (1992) defines calcurmolite more like a group of minerals having in common the presence of calcium, molybdenum, uranium and water. This assumption is explained by the discrepancies of the observed physical properties and variation in the powder X-ray diffraction patterns. The same diversity is found in the chemical formula reported by different studies (Rudnitskaya 1959; Fedorov 1963; Skvortsova et al. 1969; Deliens 1992; Sidorenko et al. 2005 and Dal Bo 2018). In the present work, the chemical formula is similar to the one reported by Dal Bo (2018) for calcurmolite from Rabejac $Ca(UO_2)_3(MoO_4)_2(OH)_4(H_2O)_8$. The difference in the water content can be due to the inaccuracy of the measurement in our study. Nevertheless, a variation in the amount of water or calcium seems highly possible considering the topology of the calcium–water layer and the disorder, especially along the stacking direction, observed in the diffraction data. It can probably occur without disturbing the topology of the uranium molybdenum layer and might be an explanation for the differences in the powder X-ray patterns reported in the literature.

6. Conclusions

The structure of calcurmolite can be considered complex regarding the topology and due to presence of commensurate/incommensurate modulations. The quality of the current data set does not allow differentiation between commensurate or incommensurate modulation but gives an insight of the structure for the first time. Although, the necessity of using the crenel-like (discontinuous) modulation functions indicates that the structure is close to be incommensurately modulated. Calcurmolite is similar to the Ba uranyl–molybdate baumoite, which was shown to be incommensurately modulated, having the same structural sheets, with U : Mo ratio equal to 3 : 2.

Tab. 3 Positional parameters for calcurmolite (SSG *P*1(α00)0)

atom	*harm.*	*x/a*	*y/b*	*z/c*	*Uiso [Å²]*	*Delta/Occ. Delta*	*x4⁰*
U1_1		0.5062	0.9549	0.3733	0.0164(4)	0.6	0.4
Mo1_1		–	–	–	0.0164(4)	0.4	0.9
	s,1	0	0	–0.0158(5)			
	c,1	0	0	0.0171(5)			
U1_2		–0.4966(16)	–0.9602(5)	–0.3912(3)	0.0164(4)	0.6	0.5989(6)
Mo1_2		–	–	–	0.0164(4)	0.4	0.0989(9)
	s,1	0	0	–0.0087(4)			
	c,1	0	0	0.0059(5)			
U2_1		0.7517(19)	0.9404(6)	0.0800(4)	0.0164(4)	0.6	0.5982(8)
Mo2_1		–	–	–	0.0164(4)	0.4	1.0982(11)
	s,1	0	0	–0.0209(5)			
	c,1	0	0	–0.0296(5)			
U2_2		–0.8693(17)	–0.9754(6)	–0.1270(3)	0.0164(4)	0.6	0.5498(11)
Mo2_2		–	–	–	0.0164(4)	0.4	–0.280(2)
	s,1	0	0	0.0078(4)			
	c,1	0	0	0.0022(5)			
O5a_1		1.123(3)	0.9597(5)	0.2324(5)	0.075(3)	0.4	1.2467(16)
O5a_2		–0.948(4)	–0.93(1)	–0.2544(5)	0.075(3)	0.4	0.018(2)
O5b_1		0.330(3)	0.9182(5)	0.2265(5)	0.075(3)	0.4	0.9296(12)
O5b_2		–0.317(3)	–0.9383(5)	–0.2609(6)	0.075(3)	0.4	0.1708(15)
O5c_1		0.602(3)	0.8865(5)	0.2231(6)	0.075(3)	0.4	0.4383(15)
O5c_2		–0.573(3)	–0.9107(5)	–0.2438(6)	0.075(3)	0.4	0.7681(17)
O5d_1		0.515(3)	0.9107(5)	0.2291(6)	0.075(3)	0.2	0.7037(13)
O5d_2		–0.527(3)	–0.9321(5)	–0.2616(6)	0.075(3)	0.2	0.3868(16)
						Occ.	
O1a_1		0.006(2)	0.2122(6)	0.374(2)	0.075(3)	1	
O1a_2		–0.032 (1)	–0.2034(6)	–0.422(2)	0.075(3)	1	
O1b_1		–0.002(1)	0.7229(7)	0.369(2)	0.075(3)	1	
O1b_2		0.026(1)	–0.7229(6)	–0.369(2)	0.075(3)	1	
O2a_1		0.266(1)	1.1917(7)	0.123(2)	0.075(3)	1	
O2a_2		–0.402(1)	–1.2084(7)	–0.198(2)	0.075(3)	1	
O2b_1		0.291(3)	0.6972(6)	0.056(2)	0.075(3)	1	
O2b_2		–0.343(1)	–0.7486(6)	–0.044(2)	0.075(3)	1	
O3_1		0.2167(13)	0.0220(3)	0.4328(5)	0.075(3)	1	
O3_2		–0.1301(18)	0.0119(3)	–0.4443(5)	0.075(3)	1	
O4_1		0.1171(17)	0.8914(3)	0.0179(5)	0.075(3)	1	
O4_2		–0.293(2)	–1.0016(3)	–0.0730(4)	0.075(3)	1	
Ca1_1		0.313(8)	0.351(2)	0.2608(14)	0.104(1)	0.4	
Ca1_2		–0.354(7)	–0.409(2)	–0.3018(15)	0.104(1)	0.4	
Ow1_1		–0.608(10)	0.480(3)	0.1181(19)	0.104(1)	1	
Ow1_2		0.551(16)	–0.505(4)	–0.1415(18)	0.104(1)	1	
Ow2_1		0.192(9)	0.463(3)	0.3852(18)	0.104(1)	1	
Ow2_2		–0.136(8)	–0.479(3)	–0.4143(16)	0.104(1)	1	

Acknowledgements. Stephan Wolfsried is thanked for the microphotography of the calcurmolite specimen. This manuscript benefited from the construction reviews of two referees including Aaron Lussier as well as from the comments of the handling editor František Laufek. This research was supported by the project No. LO1603 under the Ministry of Education, Youth and Sports National sustainability program I of Czech Republic to JP and GS, and OPVV project (CZ.02.1.01/0.0/0.0/16_026/0008459) to RS. This work was also supported by Operational Programme Research, Development and Education financed by European Structural and Investment Funds and the Czech Ministry of Education, Youth and Sports (Project No. SOLID21 CZ.02.1.01/0.0/0.0/16_019/0000760), using instruments of the ASTRA laboratory established within the Operation program Prague Competitiveness – project CZ.2.16/3.1.00/24510.

Electronic supplementary material. Supplementary original crystallographic information file (*cif*) for calcurmolite is available online at the Journal web site (*http://dx.doi.org/10.3190/jgeosci.297)*.

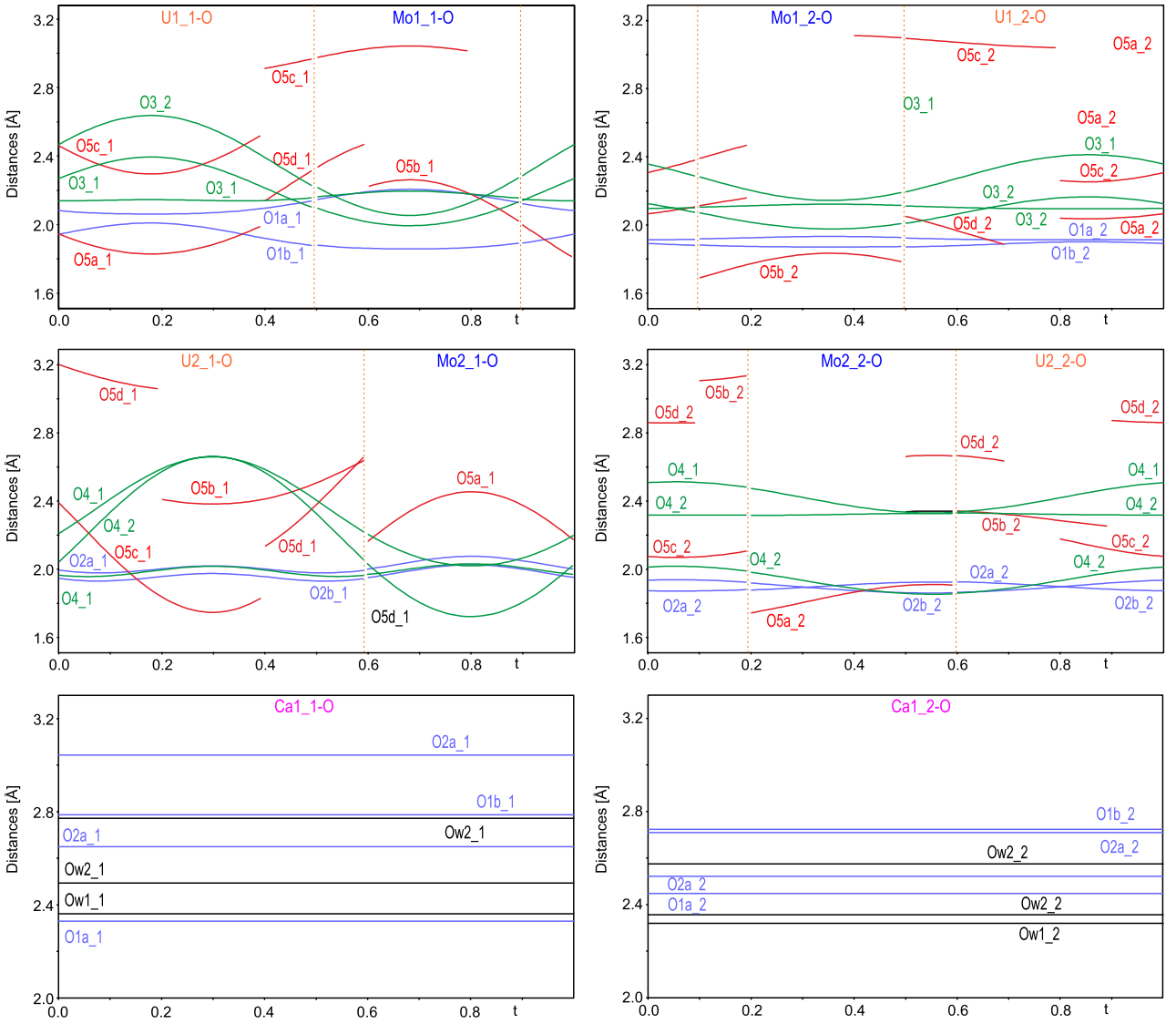

Fig. 9 The cations–oxygen distances (in Å) in the structure of calcurmolite.

References

Boullay P, Palatinus L, Barrier N (2013) Precession Electron Diffraction Tomography for solving complex modulated structures: the case of $Bi_5Nb_3O_{15}$. Inorg Chem 52: 6127−6135

Burns PC (2005) U^{6+} minerals and inorganic compounds: insights into an expanded structural hierarchy of crystal structures. Canad Mineral 43: 1839–1894

Dal Bo F, Hatert F, Philippo S (2018) Supergene uranyl mineralization of the Rabejac Deposit, Lodève, France. Minerals 8: 414

Deliens M (1992) Etude comparative des calcurmolites de Rabejac (Lodève, Herault, France) et de l'Union Sovietique. Ann Soc Geol Belg 115: 91–97

Elliot P, Plášil J, Petříček V, Čejka J, Bindi L (2019) Twinning and incommensurate modulation in baumoite, $Ba_{0.5}[(UO_2)_3O_8Mo_2(OH)_3](H_2O)_{\sim 3}$, the first natural Ba uranyl molybdate. Mineral Mag 83: 507–514

Fedorov OV (1963) Second find of calcium uranium molybdate in the USSR. Zap Vsesojuz mineral Obshch 92: 464–465 (in Russian)

Frost RL, Čejka J, Dickfos MJ (2008) Raman and infrared spectroscopic study of the molybdate-containing uranyl mineral calcurmolite. J Raman Spectrosc 39: 779–785

Hawthorne FC, Schindler M (2008) Understanding the weakly bonded constituents in oxysalt minerals. Z Kristallogr 223: 41–68

Krivovichev SV, Burns PC (2000a) Crystal chemistry of uranyl molybdates. I. The structure and formula of umohoite. Canad Mineral 38: 717–726

Krivovichev SV, Burns PC (2000b) Crystal chemistry of uranyl molybdates. II. The structure and formula of iriginite. Canad Mineral 38: 847–851

Krivovichev SV, Burns PC (2001a) Crystal chemistry of uranyl molybdates. III. New structural themes in the structures of $Na_6[(UO_2)_2O(MoO_4)_4]$, $Na_6[(UO_2)(MoO_4)_4]$ and $K_6[(UO_2)_2O(MoO_4)_4]$. Canad Mineral 39: 197–206

Krivovichev SV, Burns PC (2001b) Crystal chemistry of uranyl molybdates. IV. Crystal structures of $M_2[(UO_2)_6(MoO_4)_7(H_2O)_2]$, M = Cs, NH_4. Canad Mineral 39: 207–214

Krivovichev SV, Burns PC (2002a) Crystal chemistry of rubidium uranyl molybdates: crystal structures of $Rb_6(UO_2)(MoO_4)_4$, $Rb_6(UO_2)_2O(MoO_4)_4$, $Rb_2(UO_2)(MoO_4)_2$, $Rb_2(UO_2)_2(MoO_4)_3$ and $Rb_2(UO_2)_6(MoO_4)_7(H_2O)_2$. J Solid State Chem 168: 245–258

Krivovichev SV, Burns PC (2002b) Crystal chemistry of uranyl molybdates. VI. New uranyl molybdate units in structures of $Cs_4[(UO_2)_3Mo_3O_{14}]$ and $Cs_6[(UO_2)(MoO_4)_4]$. Canad Mineral 40: 201–209

Krivovichev SV, Burns PC (2002c) Crystal chemistry of uranyl molybdates. VII. Iriginite-type polyhedral sheet in the structure of $(UO_2)Mo_2O_7(H_2O)_2$. Canad Mineral 40: 1571–1577

Krivovichev SV, Burns PC (2002d) Synthesis and crystal structure of $Ag_6[(UO_2)_3O(MoO_4)_5]$: a novel sheet of triuranyl clusters and MoO_4 tetrahedra. Inorg Chem 41: 4108–4110

Krivovichev SV, Plášil J (2013) Mineralogy and crystallography of uranium. In: Burns PC, Sigmon GE (eds) Uranium: From Cradle to Grave. Mineralogical Association of Canada Short Courses 43: pp 15–119

Krivovichev SV, Finch R, Burns PC (2002) Crystal chemistry of uranyl molybdates V. Topologically different uranyl molybdate sheets in structures of $Na_2[(UO_2)(MoO_4)_2]$ and $K_2[(UO_2)(MoO_4)_2](H_2O)$. Canad Mineral 40: 193–200

Palatinus L, Chapuis G (2007) SUPERFLIP – a computer program for the solution of crystal structures by charge flipping in arbitrary dimensions. J Appl Crystallogr 40: 786–790

Palatinus L, Petříček V, Corrêa CA (2015a) Structure refinement using precession electron diffraction tomography and dynamical diffraction: theory and implementation. Acta Crystallogr A71: 235–244

Palatinus L, Corrêa CA, Steciuk G, Jacob D, Roussel P, Boullay P, Klementová M, Gemmi M, Kopeček J, Domeneghetti MCh, Cámara F, Petříček V (2015b) Structure refinement using precession electron diffraction tomography and dynamical diffraction: tests on experimental data. Acta Crystallogr B71: 740–751

Palatinus L, Brázda P, Jelínek M, Hrdá J, Steciuk G, Klementová M (2019) Specifics of the data processing of precession electron diffraction tomography data and their implementation in the program PETS2.0. Acta Crystallogr B75: 512–522

Petříček V, Dušek M, Palatinus L (2014) Crystallographic computing system JANA2006: general features. Z Kristallogr 229: 345–352

Petříček V, Eigner V, Dušek M, Čejchan A (2016) Discontinuous modulation functions and their application for analysis of modulated structures with the computing system JANA2006. Z Kristallogr 231: 301–312

Pouchou JL, Pichoir F (1985) "PAP" (φρZ) procedure for improved quantitative microanalysis. In: Armstrong JT (ed) Microbeam Analysis. San Francisco Press, San Francisco, pp 104–106

Rudnitskaya LS (1959) Calcium molybdate of uranium. Yadernoe Gor I Reak Met 3: 160–161

Sidorenko GA, Chistyakova NI, Chukanov NV, Naumova IS, Rassulov VA (2005) Calcurmolite: new data on chemical composition and constitution of the mineral. New Dat Min M 40: 29–36

Skvortsova KV, Kopchenova EV, Sidorenko GA, Kuznetsova NN, Dara AD, Rybakova LI (1969) Calcium–sodium uranomolybdates. Zap Vsesojuz mineral Obshch 98: 679–688 (in Russian)

Steciuk G, Boullay P, Pautrat A, Barrier N, Caignaert V, Palatinus L (2016) Unusual relaxor ferroelectric behavior in stairlike aurivillius phases. Inorg Chem 55: 8881–8891